Demonstrating Structural Integrity Under Challenging Load And Material Conditions

Chris Timbrell[1], Ramesh Chandwani[1 *] and Ma Chunlei[2]

[1]Zentech International Ltd., 590B Finchley Road, London NW11 7RX, UK

[2]Consys Group Ltd., Rm 504 Liqin Plaza, 1885 Duhui Rd, Minhang Dist., Shanghai, PRC 201108

* Corresponding author : Ramesh@zentech.co.uk

Keywords: Structural integrity, load systems, crack growth, residual life.

Abstract. Since the industrial revolution when a German mining engineer August Wohler first studied the frequent breaking of chains causing several casualties and developed the concept of what we now know as the S-N curve, many experimental, theoretical and software-aided simulation techniques have been developed to study ageing material behaviour and to design new materials. Over time the demands placed on new materials have required operation under more severe temperatures and loads in order to conserve natural resources and minimise emissions.

Fracture mechanics based finite element algorithms to simulate 3D cracks in components / structures have proved very useful in assessing the residual life and developing repair and maintenance strategies as mandatorily required by various licensing authorities for the continuous operation of infrastructure projects in Aerospace, Power, Transportation, Oil and Chemical industries under the ever more demanding operating conditions. Here one such software tool for crack simulation of industrial applications is presented with examples including combined fatigue and time dependent crack growth under thermo-mechanical loading including hold-time and weld defect assessment with inclusion of dis-similar materials.

Introduction

Fatigue failure is one of the most significant modes of failure and to predict the fatigue life of a structure requires full knowledge of both the load history and the material behaviour. Material strength is affected not only by cyclic loading but also by the environmental conditions surrounding the structure. Failures may also occur under sustained loads and high temperatures due to creep-fatigue. Also, boundary conditions such as sliding and rolling contact may also affect the fatigue life. Although in many industrial Codes of Practice, the structural fatigue life assessment procedures are still based on S-N curves and cumulative damage theories, efforts have been made to introduce improved equations to take into consideration such factors affecting respective industries. It is now accepted that crack like flaws exist not only in welded structures but also in all materials especially metallic and composites. With the help of high resolution NDT tools one is able to measure such defects at microstructural level. Much effort is being made to simulate the growth of 3D cracks at microstructural level using finite element based algorithms. However, due to the random nature of granular structure, presence of cavities, non-linear effect of ductility / plasticity, crack-tip constraint, loading and environment, etc., at the microstructural level, it is not possible to generalise the behavior and develop a unified fracture mechanics theory based on continuum mechanics principles to assess the full fatigue life [1].

Much of the current work on assessment of residual life and integrity of a structure is still based on linear elastic fracture mechanics (LEFM) principles due to the assumption that the plastic zone is small and constraint along the crack front is high. The Zencrack [2] software is most often used for crack growth studies under these assumptions. However, more complex behaviour and growth laws can be modelled for elastic-plastic crack tip models using user subroutines. For example, crack-tip models such as UNIGROW, Antolovich-Saxena and Kujawski-Ellyin [3,4,5] have been successfully used to simulate 3D crack propagation using Zencrack.

In this paper we concentrate on some of the issues related to fatigue crack growth at low temperature and the analogies that can be used in high temperature cases. Some examples are provided of high temperature defect analysis for stationary and growing cracks. A further example demonstrates how the interaction of multiple material properties can be addressed for a defect at a weld location.

Stationary cracks and fatigue crack growth at low temperature

In pure linear elastic static loading at low temperature, the stress intensity factor K describes the stress field at the crack tip. As the load magnitude increases, the amount of plasticity increases as shown schematically in Fig. 1.

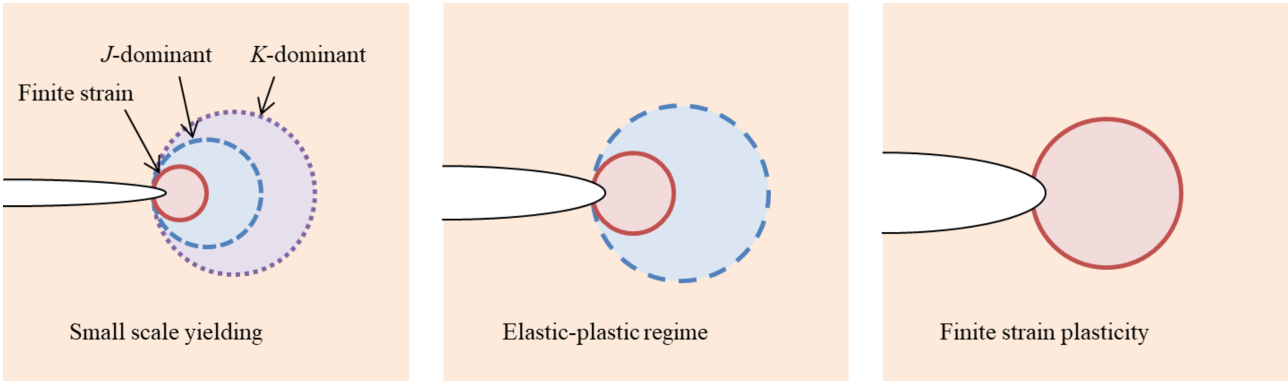

Fig. 1 – Schematic of crack tip zones for plasticity

In the small-scale yielding case both K and J characterize the crack tip conditions with a K-dominant zone extending beyond the J-dominant zone. Very close to the crack tip the strain is finite. As the load further increases to the elastic-plastic regime there is no longer a K-dominant region but the J-dominant zone still exists. Upon further loading and large scale yielding, there is no K or J dominant zone and a single parameter approach is not valid. In this regime a two-parameter fracture mechanics approach can be used with elastic T-stress, Q stress and the $A2$ parameter being considered as possible second parameters. This is not a subject for further discussion here but the plasticity scenario serves to help when considering the creep scenario.

At low temperatures, fatigue crack growth is a time independent process which is usually assessed via the stress intensity factor (K), energy release rate (G), or J-integral (J) under the assumption of small scale yielding. The evaluation of a single parameter that describes conditions at the crack tip is coupled with the load history and a crack growth law to allow evaluation of the crack growth rate, da/dN. In this context the load history must be a sequence of fatigue cycles, each having a range of loading, for example resulting in a range of stress intensity factor, $\Delta K = K_{max} - K_{min}$. For 3D cracks the evaluation of the fracture mechanics parameter must take place at multiple points along the crack front to allow a range of da values to be calculated over an increment dN in the load cycle history. The crack growth law may be a function of a number of parameters including stress ratio, R, load frequency, load cycle waveform and temperature. Typical examples are the Paris law, Eq. 1, and the Hartman-Schijve law, Eq. 2. [6] provides a review of many fatigue crack growth laws. But within this "low temperature" environment there is no consideration required of creep and thermally activated environmental effects.

$$\frac{da}{dN} = C(\Delta K)^n \tag{1}$$

$$\frac{da}{dN} = \frac{C(\Delta K - \Delta K_{th})^n}{(1-R)K_c - \Delta K} \tag{2}$$

where:

ΔK	= stress intensity factor range
ΔK_{th}	= threshold stress intensity factor range
K_c	= plane stress fracture toughness
a	= crack size
N	= load cycles
C, n	= temperature dependent material parameters
R	= stress ratio

Stationary cracks and fatigue crack growth at high temperature

At high temperatures, typically above 30-50% of the material melting temperature, the mechanisms of fracture become time dependent rather than cycle dependent and are affected by creep and environment with corrosion and oxidation playing a part in the crack growth in addition to effect of creep strain development. In this regime a crack may grow if the load is held constant for a period of time. Cycle effects may still exist within the loading sequence however, and crack growth is then a mixture of high temperature time dependent growth and cyclic effects.

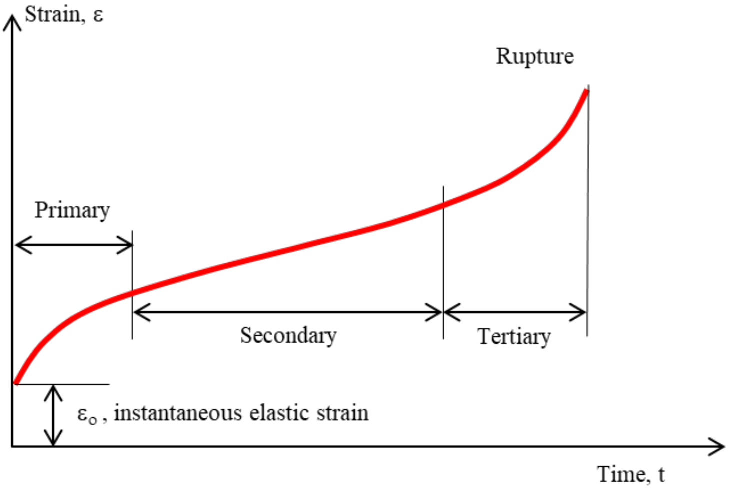

Fig. 2 – Typical strain vs time creep curve

Creep behaviour is usually described in three phases as shown schematically in Fig. 2. In primary creep the creep resistance increases with strain leading to a decreasing creep strain rate. In secondary creep there is a balance between work hardening and recovery processes leading to a constant creep rate. In tertiary creep there is an accelerating creep rate due to the accumulating damage leading to creep rupture.

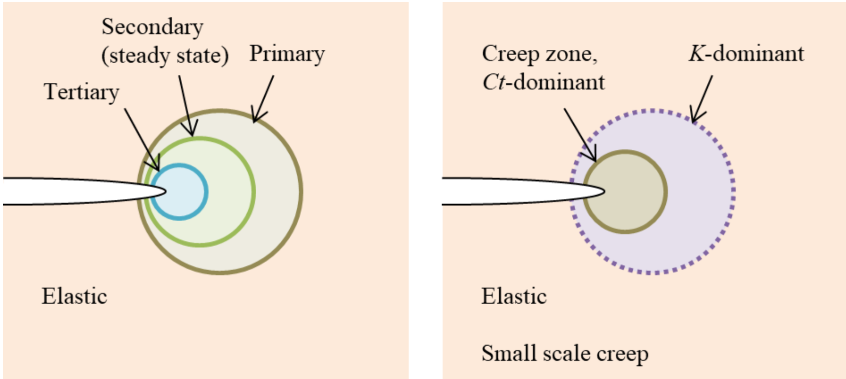

Fig. 3 – General regions ahead of the crack under creep conditions and the small scale creep regime

At high temperatures the stress field ahead of a crack evolves in a complex manner. Immediately ahead of the crack there exist zones of tertiary, secondary and primary creep surrounded by elastic material, Fig. 3. If the inelastic creep deformation zone near the crack-tip remains small compared to the crack size, stress intensity factor *K* remains the controlling parameter. This is the special case of small scale creep in which the *K*-dominant region outside the creep zone is analogous to the *K*-dominant zone for the small scale yielding case (Fig. 1).

As time progresses the stress state constantly changes. Blunting of the crack tip due to relaxation in the stress field tends to slow down crack growth whereas build-up of creep damage via formation, growth and coalescence of microvoids tends to speed up crack growth.

No single parameter can characterize all of the possible stress states.

At very high temperatures however, limitations of the *K*-dominant LEFM assumption can become apparent as the inelastic zone increases causing significant non-linear deformations to develop within the primary, secondary and tertiary regions.

Plasticity and creep are often represented by similar power laws with rate terms in the creep equation replacing rate independent terms in the plasticity equation. The similarity in the stress fields is shown in Table 1.

*C** is the (steady state) equivalent in creep to *J* in plasticity. The *C**-integral can be defined in a similar way to the *J*-integral which was originally defined in [7]. For the *C**-integral, rate terms are used in place of the original strain and displacement terms, Fig. 4. The path independency of the *C**-integral only applies when steady state conditions are prevailing i.e. the creep strain rates are much larger than the elastic strain rate in the body. This will be true after long times and when the remote load is constant. For general creep the term *Ct* is used in place of *C** to indicate that the stress magnitude depends on time. The *Ct* value is calculated using the same integral as *C** but the contour must be taken very close to the crack tip. This general form of the integral is path dependent.

Table 1 – Correspondence between plasticity and creep

Plasticity	Creep
Strain: $$\frac{\varepsilon}{\varepsilon_o} = \frac{\sigma}{\sigma_o} + \alpha\left(\frac{\sigma}{\sigma_o}\right)^n$$	Strain rate: $$\dot{\varepsilon} = \dot{\varepsilon}^{el} + \dot{\varepsilon}^{cr} = \varepsilon_o + \dot{\varepsilon}_o\left(\frac{\sigma}{\sigma_o}\right)^n$$
HRR (Hutchinson, Rice, Rosengren) stress field at the crack tip: $$\sigma_{ij}(r,\theta) = \sigma_o\left(\frac{J}{\alpha\varepsilon_o\sigma_o I_n r}\right)^{\frac{1}{n+1}} g_{ij}(n,\theta)$$	RR (Riedel-Rice) stress field at the crack tip: $$\sigma_{ij}(r,\theta) = \sigma_o\left(\frac{C(t)}{\dot{\varepsilon}_o\sigma_o I_n r}\right)^{\frac{1}{n+1}} g_{ij}(n,\theta)$$ For steady state creep, C^* replaces $C(t)$: $$\sigma_{ij}(r,\theta) = \sigma_o\left(\frac{C^*}{\dot{\varepsilon}_o\sigma_o I_n r}\right)^{\frac{1}{n+1}} g_{ij}(n,\theta)$$

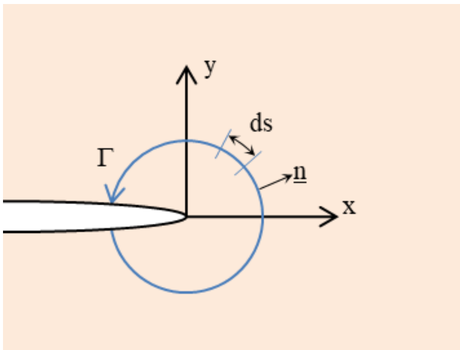

$$J = \int_\Gamma \left[W dy - T_i \frac{\partial u_i}{\partial x} ds\right] \qquad W = \int_0^\varepsilon \sigma_{ij} d\varepsilon_{ij} \qquad T_i = \sigma_{ij} n_j$$

$$C^* = \int_\Gamma \left[\dot{W} dy - T_i \frac{\partial \dot{u}_i}{\partial x} ds\right] \qquad \dot{W} = \int_0^{\dot{\varepsilon}} \sigma_{ij} d\dot{\varepsilon}_{ij}$$

where:
W = strain energy density
$\dot{W}$ = strain energy density rate
u_i = displacement vector components
$\dot{u}_i$ = displacement rate vector components
T_i = components of the traction vector
ds = length increment along Γ
n = outward normal along Γ

Fig. 4 – Correspondence between *J*-integral and *C**-integral definitions

Time dependent crack growth experiments performed at high temperatures combine two effects, namely creep and environmental processes such as oxidation and corrosion. For a given material and temperature, one process may dominate over the other. This is one of the reasons why different parameters such as stress intensity factor, *K*, or the *C**-integral or *Ct*-integral have been used by different researchers to correlate with experimental data.

Under cyclic loading conditions at elevated temperatures, conditions governing the appropriate characterising parameter very much depend on the cycle time T_{cycle} (duration of the fatigue cycle) and the transition time from small scale to widespread creep. At low temperatures and high frequencies (i.e. low T_{cycle}) fatigue crack growth is cycle dependent and characterized by ΔK. Whereas at very high temperatures and very low frequencies (i.e. very high T_{cycle}) crack growth is completely time controlled.

Various researchers have concluded that the appropriate parameter to characterise crack growth would depend on the environmental sensitivity of the material and its creep ductility.

It is therefore suggested that that time dependent crack growth may be grouped in two categories in which it occurs either by brittle or ductile mode.

In a brittle mode, the crack growth takes place essentially in a continuous manner along the grain boundary through a grain sliding mechanism. An aggressive environment would accelerate the crack growth rate and the effect of the crack tip stress relaxation due to creep would not be significant. Therefore the conditions of small scale creep would apply and a linear elastic fracture mechanics parameter *K* may be used.

A ductile mode of creep crack growth will apply where micro-cracks (or voids) initiate in front of the crack-tip and coalesce. Therefore crack growth would occur due to the accumulation of creep damage coalescing with the main crack. In this case the creep zone is relatively large and the *K* field is not valid. The *Ct*-integral or *C**-integral would apply.

Creep-fatigue crack growth

The approach often used for calculating the combined effect of fatigue and time dependent crack growth is a linear summation through the load cycle of the separate fatigue and time contributions to give the effective overall growth rate for a single load cycle (e.g. [8], [9]):

$$\left(\frac{da}{dN}\right)_{total} = \left(\frac{da}{dN}\right)_{fatigue} + \left(\frac{da}{dN}\right)_{time} \tag{3}$$

The way in which this expression is used in the literature often relates to simple repeated loading waveforms with a single cyclic event e.g. ramp-up, hold time, and ramp-down. [10] presents a summary of approaches used by several authors. For general cases and complex loading cycles, the load history and resulting fracture mechanics parameters are defined by a series of points which do not conform to a simple waveform. A generalization must then be adopted which is able to account for major and minor cycles effects within the time history of the random load variation:

$$\left(\frac{da}{dN}\right)_{total} = \sum_{1}^{fatigue\ cycles}\left(\frac{da}{dn}\right) + \int_{load\ cycle}\left(\frac{da}{dt}\right)dt \tag{4}$$

where:

$\frac{da}{dN}$ is the effective overall growth rate for a single full load cycle,

$\frac{da}{dn}$ is the growth rate due to an individual fatigue cycle within the load cycle,

$\frac{da}{dt}$ is the instantaneous time dependent growth rate.

Summation of Eq. 4 provides the accumulated crack growth history:

$$da = \sum_{1}^{load\ cycles}\left[\left(\frac{da}{dN}\right)_{total}\right] \tag{5}$$

However, there is a range of temperatures and strain rates, especially due to environmental conditions, where strong interaction can cause a higher rate of crack growth than the mere arithmetical combination. For example:

- An aggressive environment always has a strong influence on the time dependent part of the crack growth.
- Because of the synergetic interaction between mechanical and environmental conditions the effect of loading frequency can greatly affect crack growth rate. Presence of moisture and corrosive environment due to oxygen can easily cause hydrogen embrittlement and alter metallurgical properties on both crack surfaces and ahead of the crack-tip.
- A corrosive environment can affect the threshold region of crack growth - ΔK_{th} is generally reduced.

For evaluation of the effective overall growth rate using Eq. 4, it is required that *K* is evaluated for the fatigue law and therefore it is assumed that the time dependent law will also be a function of *K*. A time dependent growth law must be defined in addition to a fatigue growth law (such as a temperature dependent version of Eq. 1 or Eq. 2). An appropriate time dependent law may range from a simple Paris type law (Eq. 6 [11], Eq. 7 [12]) to a more complex law that embodies all the effects of corrosion, oxidation, microstructure, environment and temperature. One such law, based on a rate dependent Arrhenius law, is the COMET law, Eq. 8 [13].

$$\frac{da}{dt} = C(K)^n \tag{6}$$

$$\frac{da}{dt} = C(C_t)^n \tag{7}$$

$$\frac{da}{dt} = D(K)^n \;\&\; D = A\,e^{\left(\frac{-B}{T_C + 273.15}\right)} \tag{8}$$

where:

K, *Ct*	= stress intensity factor, *Ct*-integral
a	= crack size
t	= time
C, *D*, *n*	= temperature dependent material parameters
A, *B*	= temperature independent material parameters
T_C	= temperature in degrees Celsius

Within the high temperature simulation scenario the stress intensity factor *K* is sometimes used with or without recourse to a creep analysis. If a creep analysis is carried out, the *J*-integral is replaced by the rate equivalent *Ct*-integral which is the *C**-integral in steady state conditions. In terms of simulation to assess defects and crack growth at high temperature, a decision must be made about which parameter and methodology is appropriate depending upon the creep behavior of the material. If the material is creep brittle, then small scale creep conditions will apply and a *K*-dominant zone will exist. If the material is creep ductile, or for very long creep times for creep brittle materials, the *Ct*-integral should be used.

Integration of general loading history for creep-fatigue crack growth

In the combined fatigue and time dependent analysis framework required by Eq. 4, the crack growth integration must use information about both the raw load vs time history and the cycle counted version of that raw data. There are a number of possible approaches for the combined integration process. For example, all time integration could be carried out first over a loading cycle to give the second term on the right hand side of Eq. 4, followed by cyclic integration to give the first term on the right hand side of the equation. Account may or may not be taken of the change in crack size over the load cycle.

A more general approach taken by Zencrack is to associate each counted fatigue cycle with the time at which the maximum load level of the cycle occurs within the time history. An example is shown schematically in Fig. 5. In this method, the integration proceeds by integrating segments of the load vs time history to give *da/dt* contributions with instantaneous *da/dn* cycle contributions added as their time points are reached. The effect of increasing crack size is also accounted for during the integration process.

In a 3D crack front this integration process must be carried out separately for each node on the crack front using appropriate materials data for that particular node point. In this way, a crack may be allowed to traverse a material interface. Further, the integration process must ensure that the entire crack front advances in a consistent way i.e. the total time change at the end of a step within the integration process must be the same for all nodes on the crack front. This procedure, which is implemented in Zencrack, ensures correct prediction of the crack shape.

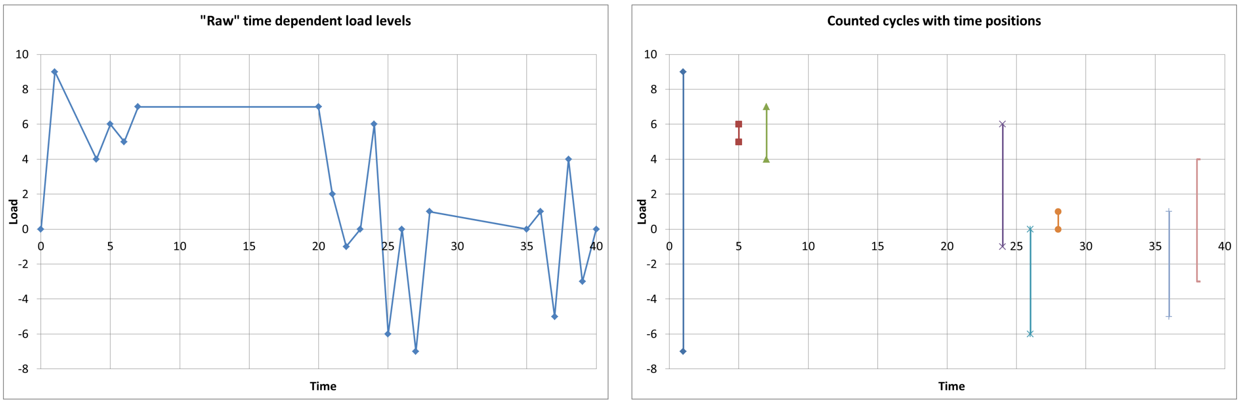

Fig. 5 – Example of "time positioned" counted cycles

Example - Creep analysis of an embedded crack in a reheater drum to calculate C*

This example is of a steel reheater drum. The model is a sector of the drum including one stub, Fig. 6. The load is constant internal pressure of 4.14MPa. The drum inner radius is 457.2mm, outer radius 541.34mm. The stub inner diameter is 31.4mm and the outer diameter 48.3mm. The analysis is performed using a creep power law, Eq. 9.

$$\dot{\bar{\varepsilon}}^{cr} = Aq^{n} \quad (9)$$

where:

$\dot{\bar{\varepsilon}}^{cr}$ = the uniaxial equivalent creep strain rate

q = the uniaxial equivalent deviatoric stress

A, n = material properties

An embedded defect of irregular shape is modelled in the drum wall (Fig. 6, Fig. 7). The defect lies on an inclined plane close to the bore of the stub. It has overall width 67.5mm and height 42.2mm. The aim of the analysis is to demonstrate the calculation of C^*. For a 3D crack of this type there is a distribution of *Ct* along the length of the crack front.

The analysis is performed using C3D20R elements in Abaqus [14]. At the crack front the elements are collapsed 20 noded brick elements. Results for two crack tip models are shown. The first uses the tip modelling method which produces a r^{-1} singularity in the stress field - this has multiple nodes at each crack tip position and the radial midside nodes at the midside position. This tip model is generally referred to as an elastic-plastic tip model. The second model does not try to enhance the stress field and uses a single node at each crack tip position, again with the midside nodes at their midside positions. The former should be more appropriate for a *Ct*-dominant zone.

In an elastic analysis to evaluate the *J*-integral the load is applied and the *J*-integral evaluated. For a creep analysis the evaluation of the steady state C^* value requires more care. The finite element solution provides the general *Ct*-integral and it becomes the responsibility of the user to determine the steady state C^* distribution. The issue then becomes: when is steady state reached? There are several things to consider:

- The C^*-integral is constant under steady state creep.
- The contour integral calculation is path independent under steady state creep. As with all contour integral evaluation, the results from the first contour are expected to be numerically least reliable.
- In steady state the creep strains continue to increase linearly with time and will be larger than the elastic strains. The simple power law creep model does not include any tertiary creep effects, so if the analysis is continued for too long, the creep strains become unrealistically high. The results shown here are for analysis time up to t=10^{6}hr.

The solution of the analysis must be reviewed with these points in mind in order to determine a whether a suitable C^* condition has been achieved.

Fig. 7 shows two key positions on the crack front that are used in the subsequent xy plots. The distance along the crack front is measured from the green point in the direction indicated. The position having the peak final *Ct* value is shown by the yellow point.

Fig. 8 and Fig. 9 show the *Ct*-integral distribution along the crack front at the end of the analyses for the r^{-1} and normal tip models respectively. It is expected that contour 1 produces least accurate results and that other contours should be path independent (if steady state has been reached). Clearly the normal tip model performs slightly worse of the two cases since contours 1 and 2 are both different than the other contours. However, not withstanding those differences, the *Ct* magnitudes and distributions for the two tip models are very similar.

Fig. 10 and Fig. 11 show the *Ct*-integral variation with time at the point having the highest final *Ct* value. In Fig. 10 the *x* axis covers the entire time period. The path dependence of the contour integral values at low times can clearly be seen. On this scale it appears that path independence is reached at around t=1000. In Fig. 11 the *x* axis is zoomed in and shows that there continues to be a small change in the *Ct* value through to the end of the analysis, although the rate of change is very low (and is exaggerated somewhat by the log scale of the plot).

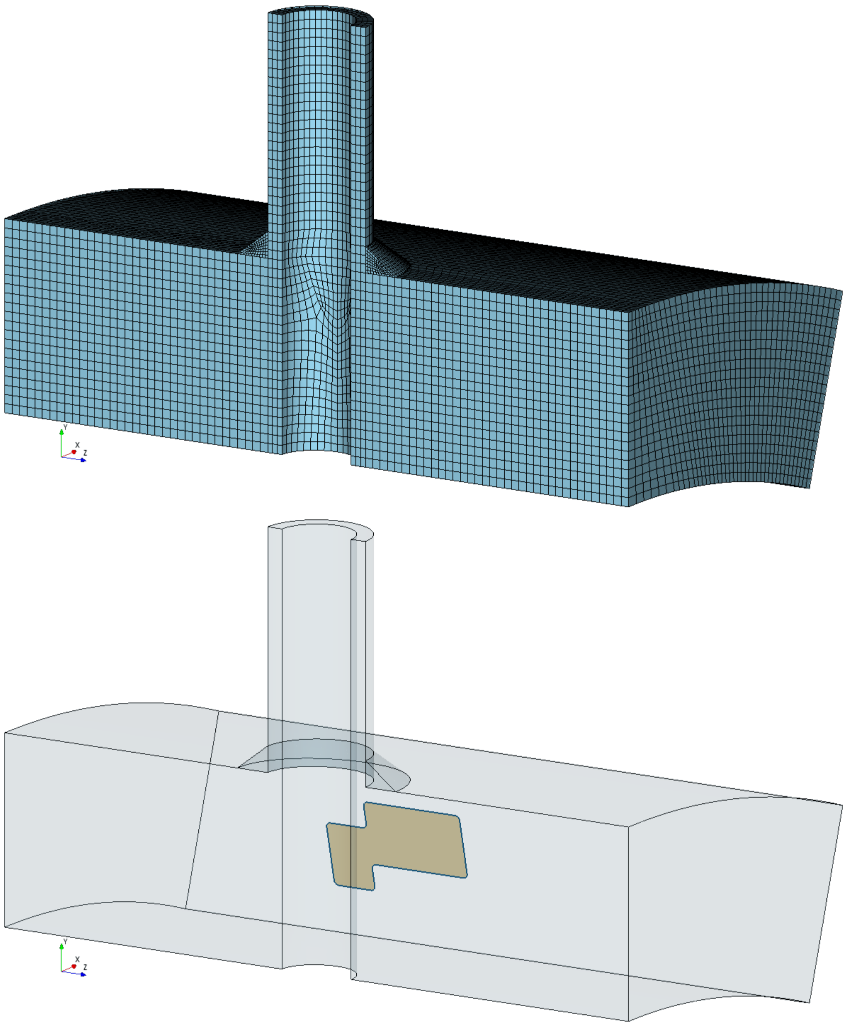

Fig. 6 – External mesh of the drum and stub and the internal embedded defect

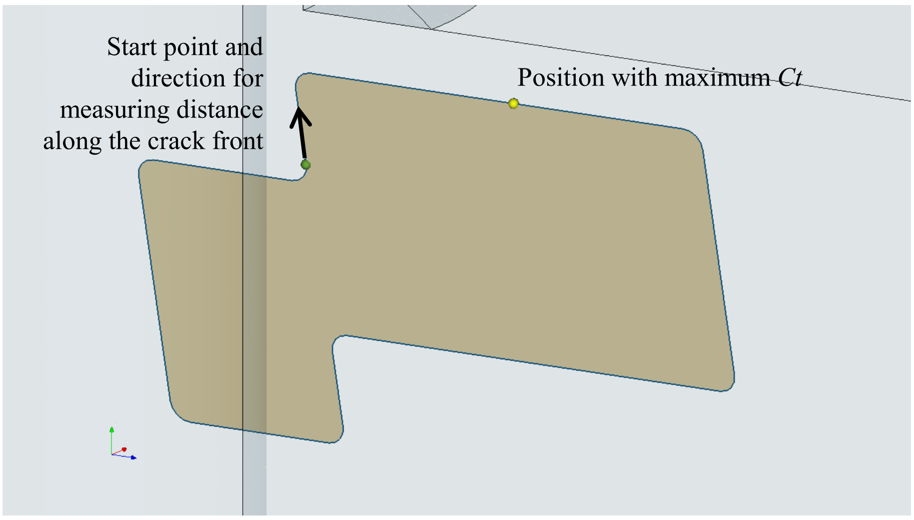

Fig. 7 – Key positions on the crack front

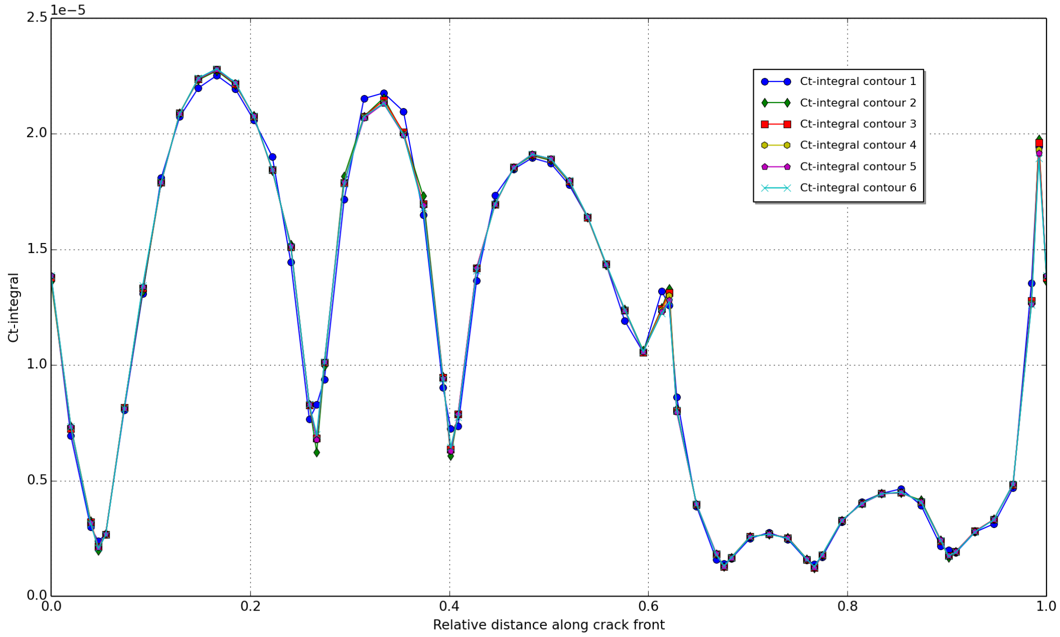

Fig. 8 – *Ct*-integral along the crack front for r^{-1} tip model, at time=1e6hr

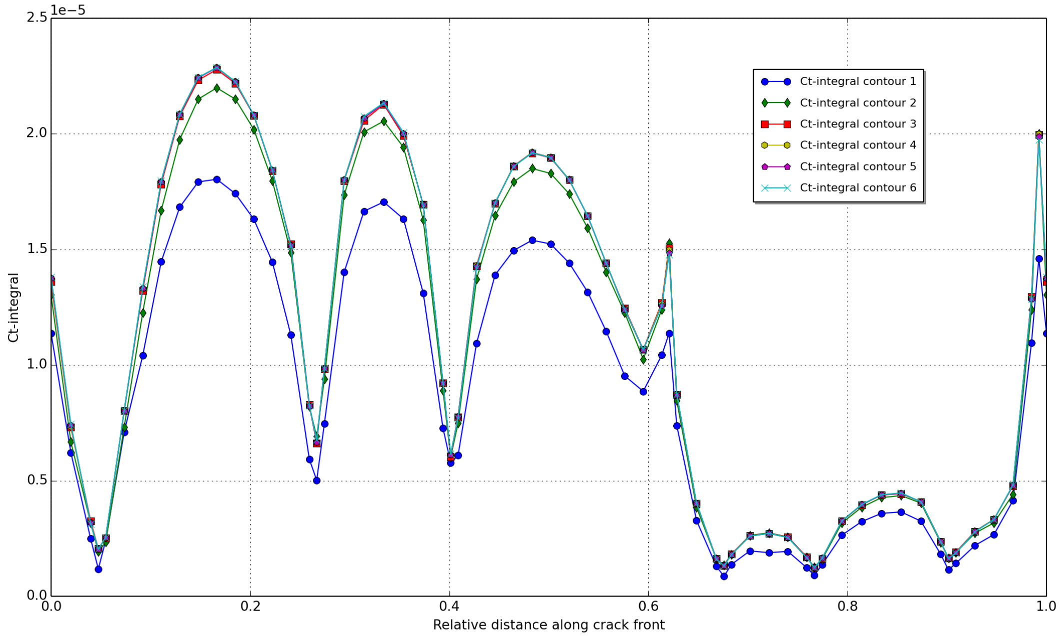

Fig. 9 – *Ct*-integral along the crack front for “normal” tip model, at time=1e6hr

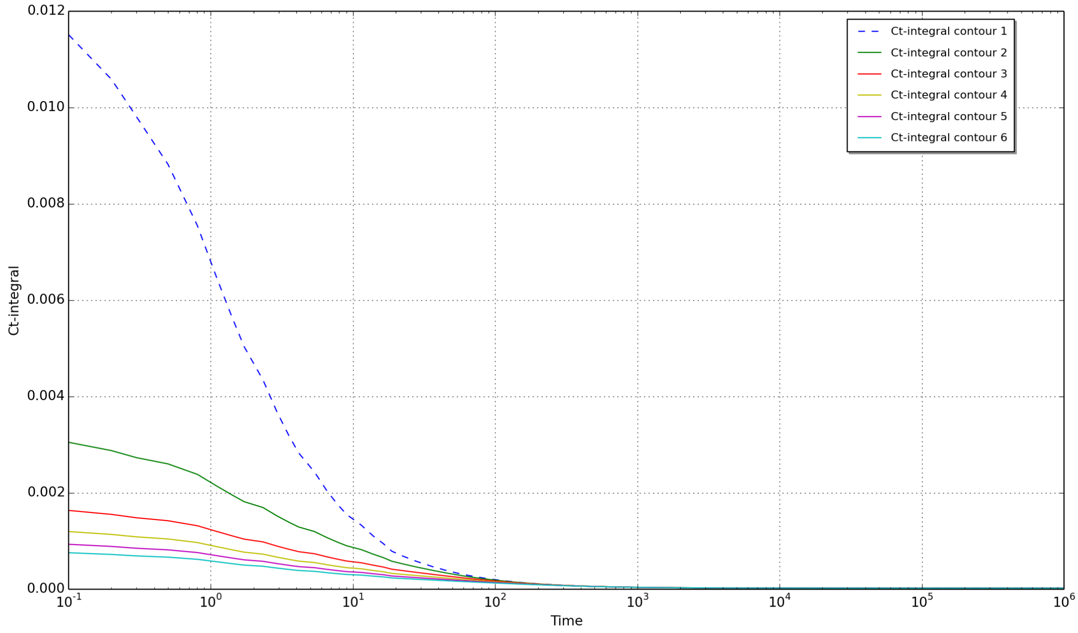

Fig. 10 – *Ct*-integral time history for position with highest final *Ct*

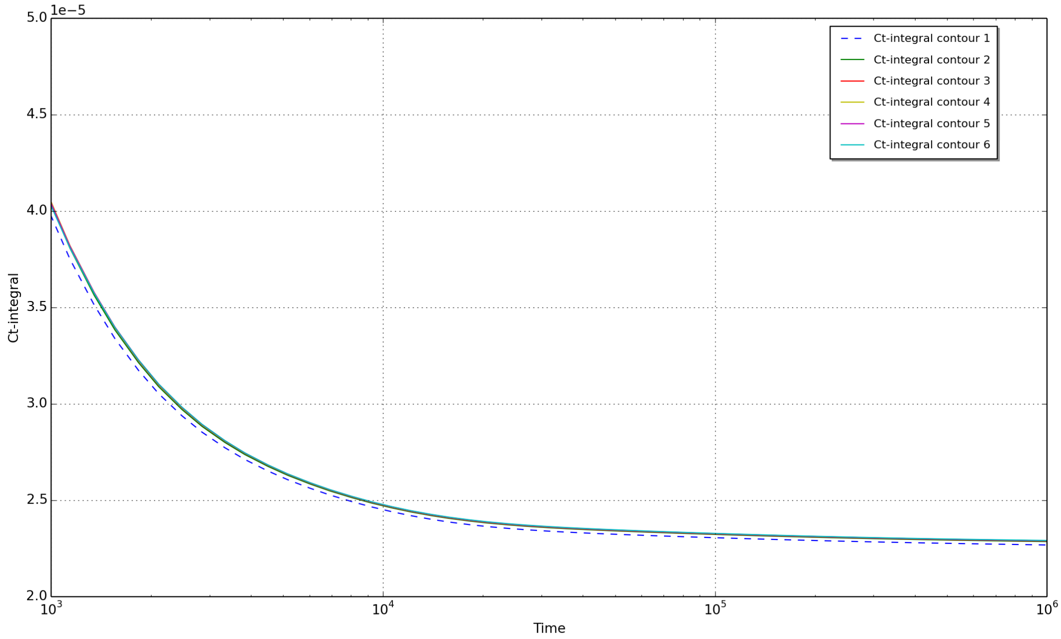

Fig. 11 – *Ct*-integral time history for position with highest final *Ct* (zoomed *x* axis)

Example - Crack growth in TMF test specimens

Fig. 12 shows the geometry of a test specimen. A starter crack is modelled at the mid-length position. This starter crack is a quarter circular corner crack of radius 0.5mm in the 7mm x 7mm square cross section.

The finite element model is a half symmetry model with the crack introduced at the symmetry plane. An uncracked Abaqus model containing C3D20 elements has the starter crack is introduced by Zencrack. The crack tip is modelled with collapsed crack front elements having quarter point nodes. The load is applied at a single point and distributed onto the cylindrical outer surface of the end of the model using a distributed coupling constraint. The load and temperature time histories are defined using *AMPLITUDE definitions. The temperature changes are applied instantaneously throughout the body (i.e. the temperature is uniform through the model at any time instant). The Abaqus *CONTOUR INTEGRAL option is used to calculate energy release rates along the crack front through the time history. The analysis uses temperature dependent Young's modulus and Poisson ratio for coarse grained RR1000. This is a high strength nickel based alloy developed by Rolls-Royce for disc applications [15]. Temperature dependent Walker coefficients are used for the fatigue law and a COMET law (i.e. Eq. 8) is used for the time dependent growth law. The crack growth is calculated using Eq. 4 and the integration procedure described earlier.

The simulations for this analysis use linear elastic modelling with temperature dependent material and crack growth laws. The crack growth laws are *K* based with growth calculations using *K* values determined from the linear elastic analyses. The high temperature effects that occur in the physical specimen are embodied within the two crack growth laws that are derived from test data correlated against *K* solutions [16]. Small scale creep conditions dominate in this high strength alloy thus making *K* a valid parameter for the simulation.

An initial cracked mesh and an analysis result showing calculated growth profiles superimposed on the geometry are shown in Fig. 13.

Several load and temperature histories were defined as part of this study with testing also being carried out. A typical load cycle is shown in Fig. 14. The aim of the process was to determine whether simulation using "standard" growth laws could be applied to predict growth in complex thermo-mechanical load cycles. More detailed comparison of the simulation and test results can be found in [16].

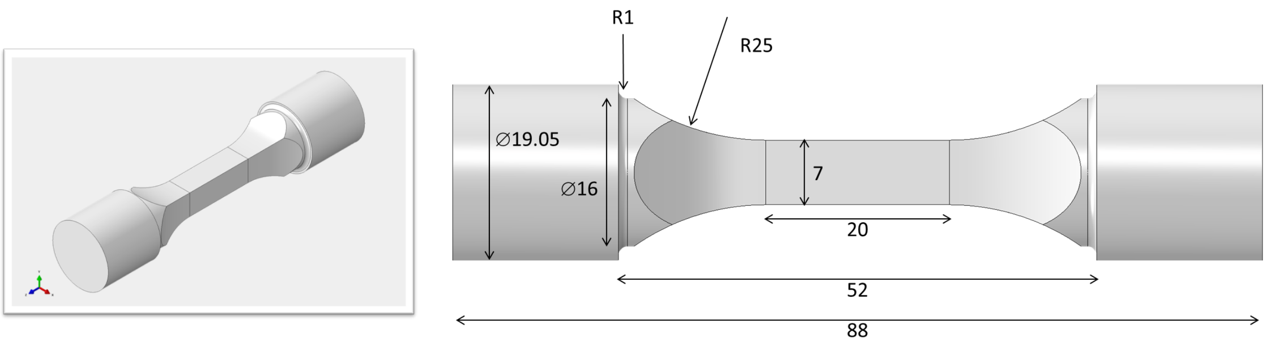

Fig. 12 – Test specimen geometry

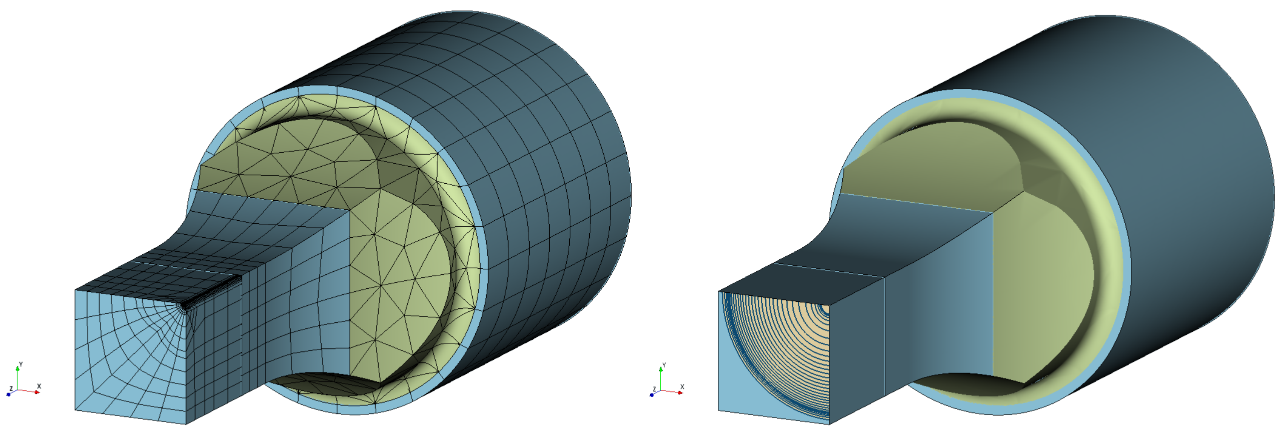

Fig. 13 – Mesh for initial crack (left) and growth profiles superimposed on the geometry (right)

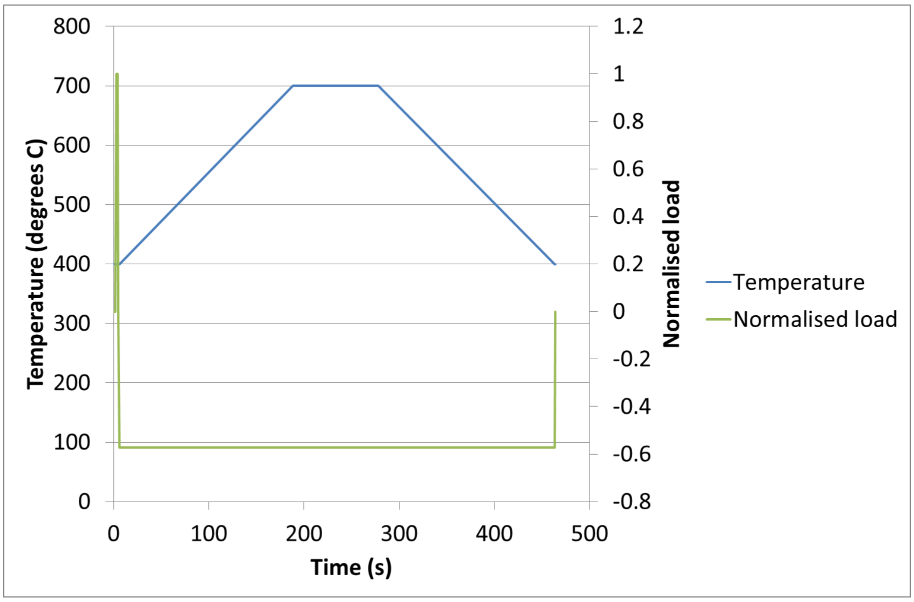

Fig. 14 – Load and temperature time history

Example - Growth of a defect across a multi-material weld zone

This example is a butt weld of structural steel pipe with OD = 57 mm and WT = 9.5 mm under a mixed loading of internal pressure of 0-758bar (R=0) at Low Frequency High Amplitude (LFHA) that occurs every hour and in between 644-758bar (R=0.85) at High Frequency Low Amplitude (HFLA) every minute (shown schematically in Fig. 15).

The pipe, weld and initial crack geometry are shown in Fig. 16. The defect is idealized as an elliptic lack of fusion defect from radiography examination. The ellipse major, minor axes lengths and inclination are: 3.6mm, 1.8mm, 10° to pipe axis. The ellipse centre is offset from the material interface at the inner wall: axial 1mm, radial 1.5mm.

The elastic material properties for the base and weld metal are different (Table 2). The crack growth properties are also different for the two active stress ratios of 0 and 0.85 (Table 3). In terms of simulation using the finite element method the former presents a difficulty in that element distributions to describe the crack front conflict with the requirement to define the material interfaces. To resolve this, both Abaqus and Zencrack user subroutines are used to allow material properties to be defined as a function of position – if a point is within the weld region, then weld properties are applied, otherwise base properties are applied. This means that the element distribution can meet the crack front requirement, with some approximation in the representation of the material interface. This is discussed in more detail in [17].

Crack growth in the radial-axial plane was calculated using Zencrack up to the point where the crack opened to the external surface (leak before break). At this point the stress intensity factor had become close to but still not reached the threshold of unstable growth (K_{Ic}) and therefore additional crack growth could be tolerated in axial direction along the pipe axis under the hoop stress. Calculated profiles for the simulation are shown in Fig. 17. For clarity a subset of the full set of profiles is shown.

A key aspect of the differences in the crack growth data is that the threshold, K_{th}, for the R=0.85 loading is much higher than for the R=0 loading. This means that as the crack grows, growth from the R=0.85 loading is not activated until K exceeds the higher threshold value of 21MPa-m$^{1/2}$. Since there is a distribution of K values along the crack front, this means that there will be a local region, where K is highest, in which the effect of the low amplitude high frequency loading is first activated. The effect of the low amplitude loading gradually extends along the crack front as the K values increase. This can be confirmed by considering four individual profiles and their K values close to the region where the crack shape starts to change. Fig. 18 and Fig. 19 confirm the expectation of the K>21 region extending and the growth increasing in those regions due to the activation of growth from the R=0.85 loading. These complex interactions between load and material properties must be accounted for within the crack growth integration scheme in order to correctly obtain this type of crack shape development.

Finally, Fig. 20 shows profiles for a simulation with only R=0 loading. The profile shape remains much more uniform with changes in shape attributed to the different material properties. These profiles also show that the analysis can be continued with two through wall defects after the leak condition is reached.

Additional load case comparison and discussion for this simulation can be found in [17].

Table 2 – Elastic properties

	Tensile Modulus of Elasticity (GPa)	Poisson Ratio
Weld	210	0.33
Base	205	0.33

Table 3 – Crack growth laws, threshold and failure (units: *da/dN* m/cycle, K MPa-m$^{1/2}$.)

	$R = 0$				$R = 0.85$			
	C	m	K_{th}	K_{Ic}	C	m	K_{th}	K_{Ic}
Weld	1.35x10^{-12}	3.6	6	65	1.13x10^{-16}	5.8	21	65
Base	1.60x10^{-14}	4.8	5.5	65	1.34x10^{-18}	7.0	21	65

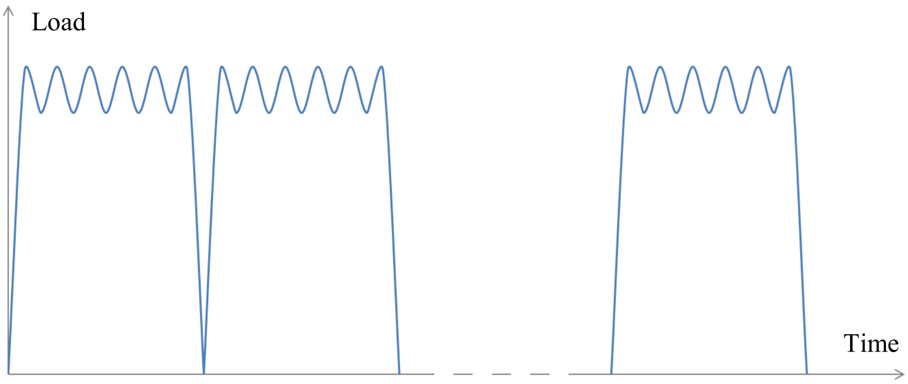

Fig. 15 – Schematic representation of load variation

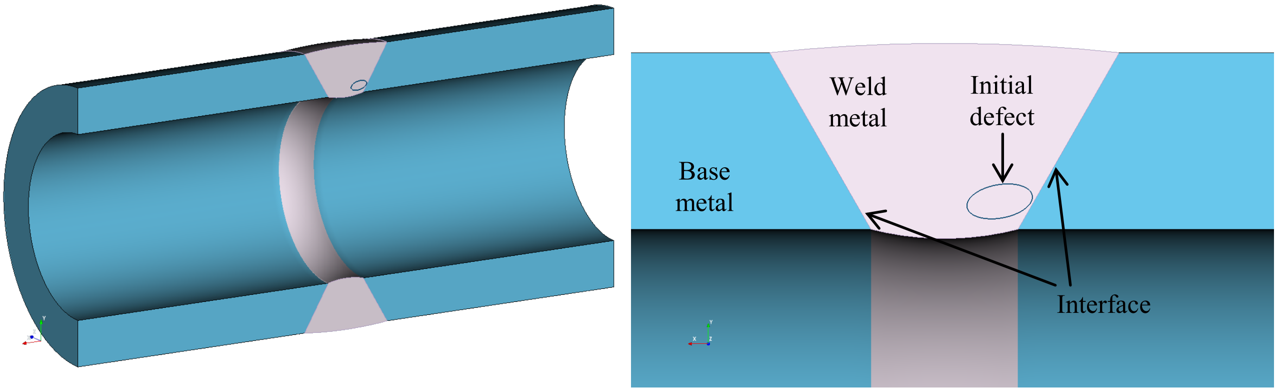

Fig. 16 – Geometry and initial crack location

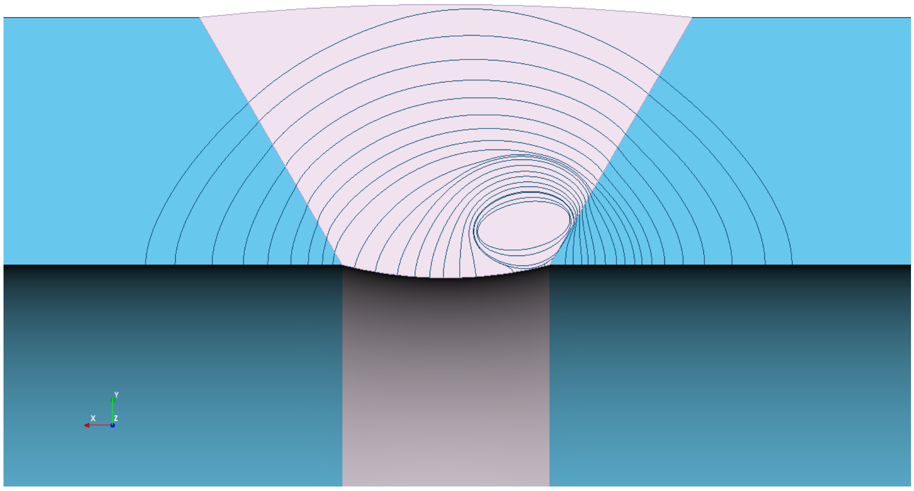

Fig. 17 – Calculated crack profiles for combined R=0 and R=0.85 loading

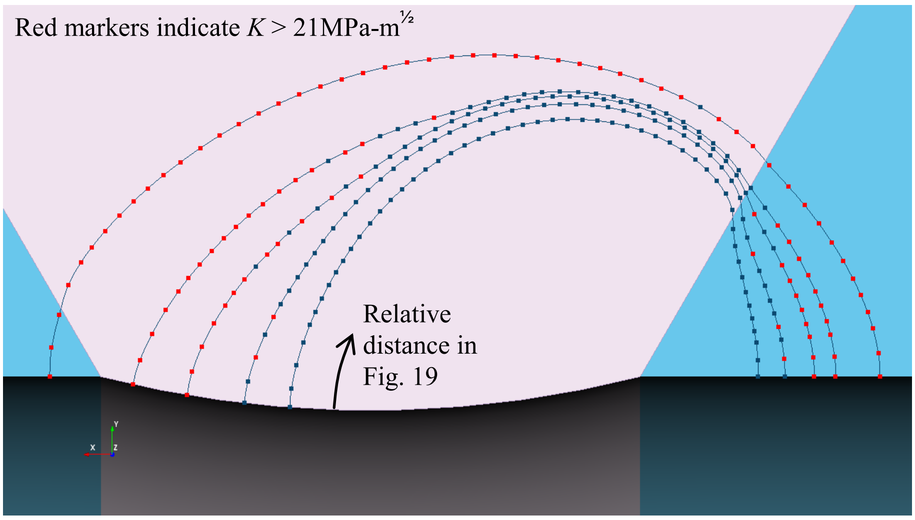

Fig. 18 – Five selected profiles - analysis steps 130, 200, 320, 368, 434

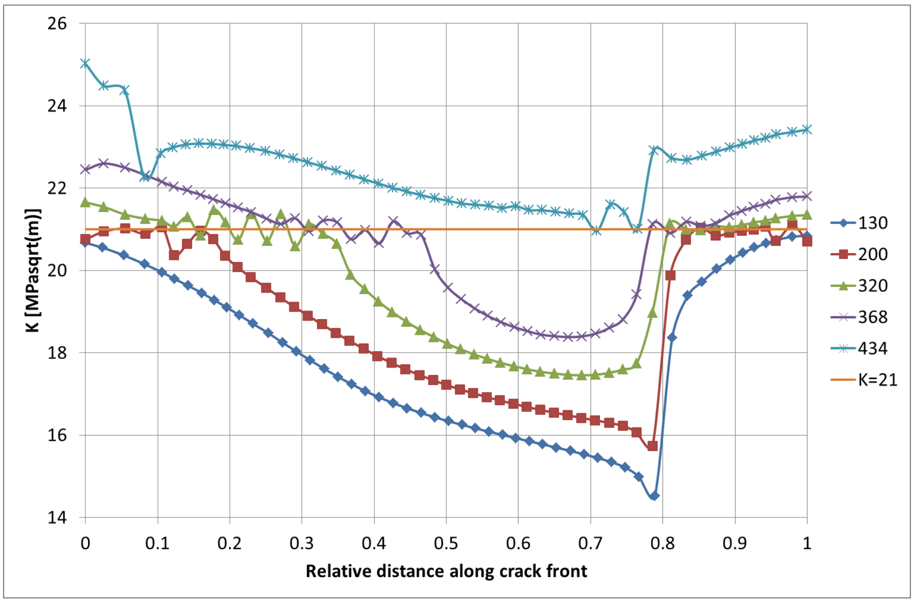

Fig. 19 – *K* values for the profiles in Fig. 18

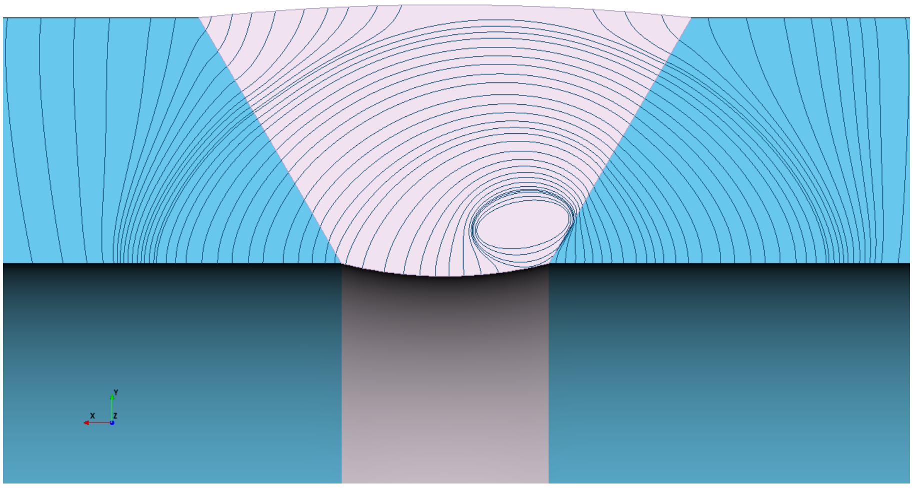

Fig. 20 – Calculated crack profiles for *R*=0 loading

Summary

Some discussion has been provided on the similarity of some aspects of creep behavior when compared to elastic-plastic behavior. In particular for simulation purposes the relationship between small scale plasticity or creep and a *K*-dominant zone compared with more widespread plasticity and creep and a *J* or *Ct* dominant zone.

These material behaviours are included as part of the framework that must be in place to solve crack simulation problems that involve complex material behavior as well as complex load histories.

Examples have been provided showing how software such as Zencrack [2], coupled with commercial finite element codes, is able to provide solutions to such problems.

References

[1] W. Cui, F. Wang, X. Huang, Towards a unified fatigue life prediction method for marine structures, Zhejiang University Press / Springer –Verlag GmbH, ISBN 978-3-642-41830-3.

[2] Zencrack, Zentech International Limited, http://www.zentech.co.uk

[3] A.H. Noroozi, G. Glinka, S. Lambert, A two parameter driving force for fatigue crack growth analysis, International Journal of Fatigue, Vol. 27 (2005) 1277-1296.

[4] S.D. Antolovich, A. Saxena, G.R. Chanani, A model for fatigue crack propagation, Engineering Fracture Mechanics, Vol. 7 (1975) 649-652.

[5] D. Kujawski, F. Ellyin, A fatigue crack propagation model, Engineering Fracture Mechanics, Vol. 20 (1984) 695-704.

[6] S.M. Beden, S. Abdullah, A.K. Ariffin, Review of fatigue crack propagation models for metallic components, European Journal of Scientific Research, Vol. 28 (2009) 364-397.

[7] J.R. Rice, A path independent integral and the approximate analysis of strain concentration by notches and cracks, Journal of Applied Mechanics, Vol. 25 (1968) 379-386.

[8] J. Gayda, T.P. Gabb, R.V. Miner, Fatigue crack propagation of nickel-base superalloys at 650C, NASA Technical Memorandum 87150, 1985.

[9] T. Nicholas, M.L. Heil, G.K. Haritos, Predicting crack growth under thermo-mechanical loading, International Journal of Fracture, Vol. 41 (1989) 157-176.

[10] C. Moura Branco, A. Sousa e Brito, J. Byrne, Life extension methodology based on creep-fatigue models, RTO AVT Workshop, Corfu, Greece, Oct 5-6 1998, in: “Qualification of Life Extension Schemes for Engine Components”, ISBN 92-837-1012-6.

[11] S. Floreen, R.H. Kane, An investigation of the creep-fatigue environment interaction in a Ni-base superalloy, Fatigue of Engineering Materials and Structures, Vol. 2 (1980) 401-412.

[12] R.M. Pelloux, Experimental and theoretical studies of creep crack growth, Air Force Office of Scientific Research Report, AFOSR-TR-84-0387, 1984.

[13] C. Timbrell, R. Chandwani, D. MacLachlan, S. Williams, A time dependent crack growth law for high temperature conditions, NAFEMS European Conference: Multiphysics Simulation, Frankfurt, Germany, Oct 16-17 2012.

[14] Abaqus, Dassault Systèmes Simulia Corp. (SIMULIA), http://www.simulia.com.

[15] M.C. Hardy, B. Zirbel, G. Shen, R. Shankar, Developing damage tolerance and creep resistance in a high strength nickel alloy for disc applications, In Proceedings of the TMS (The Minerals, Metals and Materials Society), Charlotte, NC, USA, 14–18 March 2004.

[16] C. Timbrell, R. Chandwani, S. Jacques, L. Waterhouse, A. Wisbey, S. Williams, Comparing crack growth testing and simulation results under thermo-mechanical fatigue conditions, 13th International Conference on Fracture, Beijing, China, 16-21 June 2013.

[17] M. Asadi, M. Kashani, M. Smith, C. Timbrell, R. Chandwani, A. Rodbari, A 3D crack evolution in weld metal, base metal and the transitional fusion line under a mixed fatigue loading, ESIA14–ISSI2017 (Engineering Structural Integrity Assessment 14 in conjunction with the International Symposium on Structural Integrity 2017), Manchester, UK, 16-17 May 2017.